J. Fluid Mech. (2008), *vol.* 613, *pp.* 329–356.
doi:10.1017/S0022112008003261 Printed in the United Kingdom

On internal waves generated by large-amplitude circular and rectilinear oscillations of a circular cylinder in a uniformly stratified fluid

EUGENY V. ERMANYUK AND NIKOLAI V. GAVRILOV

Lavrentyev Institute of Hydrodynamics, 630090, Novosibirsk, Russia
ermanyuk@hydro.nsc.ru

(Received 1 April 2008 and in revised form 26 June 2008)

This paper presents an experimental study of internal waves generated by circular and rectilinear oscillations of a circular cylinder in a uniformly stratified fluid. The synthetic schlieren technique is used for quantitative analysis of the internal-wave parameters. It is shown that at small oscillation amplitudes, the wave pattern observed for circular oscillations is in good agreement with linear theory: internal waves are radiated in the wave beams passing through the first and third quadrants of a Cartesian coordinate system for the clockwise direction of the cylinder motion, and the intensity of these waves is twice the intensity measured for 'St Andrew's cross' waves generated by purely horizontal or vertical oscillations of the same frequency and amplitude. As the amplitude of circular oscillations increases, significant nonlinear effects are observed: (i) a strong density-gradient 'zero-frequency' disturbance is generated, and (ii) a region of intense fluid stirring is formed around the cylinder serving as an additional dissipative mechanism that changes the shape of wave envelopes and decreases the intensity of wave motions. In the same range of oscillation amplitudes, the wave generation by rectilinear (horizontal and vertical) oscillations is shown to be by and large a linear process, with moderate manifestations of nonlinearity such as weak 'zero-frequency' disturbance and weak variation of the shape of wave envelopes with the oscillation amplitude. Analysis of spatiotemporal images reveals different scenarios of transient effects in the cases of circular and rectilinear oscillations. In general, circular oscillations tend to generate disturbances evolving at longer time scales.

1. Introduction

It has long been recognized (see e.g. Turner 1973) that internal waves play an important role in the dynamics of atmosphere and ocean, being responsible for significant transport of momentum and energy through stratified fluids. Much of our knowledge of the underlying physics of internal-wave generation, propagation, decay and interaction with the topography comes from theoretical and experimental studies of simplified generic problems. For example, investigation of internal-wave radiation by bodies undergoing small harmonic oscillations in a uniformly stratified fluid has provided a deep insight into the dynamics of topographically generated internal waves, in particular, into the non-trivial relation between the spatial structure of wave beams, geometry of the oscillating disturbance and viscosity of fluid. The phase pattern of internal-wave beams generated by a vertically oscillating cylinder in a uniformly stratified fluid has been identified in the seminal paper by Mowbray &

Rarity (1967). The energy radiated by a vibrating cylinder is known to be spread into four wave beams inclined at angle θ to the vertical, with the cylinder at the centre of this pattern known as 'St Andrew's cross' waves. The dispersion relation for internal waves in a uniformly stratified fluid relates angle θ, which is also the angle between the group velocity vector and the vertical, with the frequency of oscillations. The vector of the phase velocity is perpendicular to the vector of group velocity. Since the wavelength does not appear in the dispersion relation, the spatial structure of internal-wave beams has no length scale that might be known *a priori*. Another complication is that linear theory of ideal uniformly stratified fluid predicts infinite displacements of fluid particles along the lines tangent to the oscillating body and inclined at angle θ to the vertical (Hurley 1997). With fluid viscosity taken into account, a realistic estimate of the cross-beam distribution of the displacements of fluid particles has been obtained in Hurley & Keady (1997). However, the linear approximate solution presented in Hurley & Keady (1997) does not fulfil the no-slip condition on the body surface and therefore neglects the effect of the boundary layers on the surface of the oscillating body. The approximate solution obtained in Hurley & Keady (1997) has been confirmed by detailed quantitative measurements of internal wave patterns generated by small oscillations of circular cylinders (Sutherland *et al.* 1999, 2000). In these experiments, the amplitudes of oscillations did not exceed 20 % of the cylinder radius. Additional support to the theoretical results presented in Hurley (1997) and Hurley & Keady (1997) has been given by the measurements of forces acting on oscillating cylinders performed under conditions when both the oscillation amplitude and the thickness of boundary layers were much smaller than the diameter of the cylinders (Ermanyuk 2000; Ermanyuk & Gavrilov 2001).

Experiments with elliptic cylinders described in Sutherland & Linden (2002) have been focused on the effects related with the finite thickness of boundary layers, finite amplitude of oscillations, and some second-order wave effects, in particular, generation of the second-harmonic internal waves. Amplitude of oscillation of elliptic cylinders in Sutherland & Linden (2002) was up to 20 % of the characteristic size of the cylinders defined as the half-sum of the major and minor half-axes. Cylinders with aspect ratio of up to 3 have been used, and the ratio of the oscillation amplitude to the minor half-axis could reach 37 %, allowing us to observe significant nonlinear effects. The boundary-layer thickness was comparable with the amplitude of oscillations. In particular, Sutherland & Linden (2002) conclude that for large-amplitude oscillations 'the nonlinear dynamics involve interactions between waves and boundary layers', which deserves further studies. Also Sutherland & Linden (2002) have presented spatiotemporal images illustrating the duration of transient processes in formation of wave beams after the start-up of the oscillations. Indeed, the theoretical analysis presented in Hurley & Keady (1997) is developed for the case of steady-state harmonic oscillations. Therefore it yields no information on the duration of the transient processes. Theoretical study (Voisin 2003) of the transient processes has emphasized complicated non-trivial dynamics of internal-wave beams formation. As discussed below, nonlinear effects associated with large-amplitude oscillations are likely to introduce long time scales of the transient phenomena.

In the present paper, we describe experiments on internal-wave generation by a circular cylinder undergoing harmonic oscillations with amplitudes comparable to the radius of the cylinder. For a better understanding of the effects introduced by the boundary-generated vorticity in a real viscous uniformly stratified fluid, we study the cases of both rectilinear (horizontal and vertical) and circular oscillations. In what follows, we use the terms 'circular oscillations' and 'orbital motion' interchangeably

to denote the motion that can be represented as a sum of two orthogonal sinusoidal rectilinear oscillations of equal amplitude shifted in phase by $\pm\pi/2$. The centre of the body describes a circle while the orientation of the body remains the same (zero rotation). In principle, as long as the wave generation can be considered a linear process and the free-slip condition at the cylinder surface is assumed, there is no fundamental difference between rectilinear and circular oscillations. Both cases can be described within the framework of Hurley (1997) and Hurley & Keady (1997). However, with the no-slip condition on the cylinder surface and/or the finite oscillation amplitude taken into account, we may expect not only a quantitative but also a qualitative difference between the patterns of internal waves and currents generated by circular and rectilinear oscillations.

In a homogeneous fluid, rectilinear and circular oscillations of a circular cylinder generate essentially different mass-transfer secondary currents. Such currents are known to form four circulating cells in the vicinity of a cylinder undergoing rectilinear vibrations (see e.g. § 5.13 in Batchelor 1967), and a steady circulation around the cylinder in the case of circular oscillations (Longuet-Higgins 1970; Riley 1971). Thus, in the latter case, the mass-transfer current has a non-zero total angular momentum with respect to the centre of oscillations, whereas in the former case the total angular momentum is zero. The presence of uniform vertical density stratification hinders the formation of circulating cells and favours the formation of nearly horizontal currents. Having regard to the difference of the total angular-momentum balance, we can expect that circular oscillations of the cylinder in a uniformly stratified fluid should generate much stronger nearly horizontal mass-transfer currents as opposed to the case of rectilinear oscillations. In accordance with the dispersion relation for a uniformly stratified fluid, nearly-horizontal currents can be interpreted as 'zero-frequency' disturbances. Therefore their development after the start-up of the motion is expected to have long transient time scales.

A feature of the circular oscillations of a circular cylinder is that such motion allows us to select the direction of wave radiation. This effect was first recognized for surface waves (see Dean 1948; Ursell 1950; Ogilvie 1963). In the case of small circular oscillations of a circular cylinder fully submerged in a homogeneous fluid of infinite depth, progressive surface waves radiate in only one direction (for clockwise motion the waves radiate to the right). This effect is related with the symmetry/anti-symmetry properties of wave fields generated by vertical/horizontal oscillations of the circular cylinder. When the phase shift between vertical and horizontal oscillations is equal to $\pm\pi/2$ (i.e. for a circular orbit of the cylinder centre), the outgoing waves on one side can cancel each other. The linear analysis has been extended to the case of a two-layer fluid with an interface (Sturova 1994) and a continuous stratification with homogeneous upper and lower layers with a linearly stratified pycnocline in between (Sturova 1999). In a more general case, Sturova's (1999) results imply (personal communication) that if a circular cylinder is fully submerged in the infinitely deep homogeneous lower layer, and there exists an arbitrary stable stratification above this layer, then the orbital motion of such a cylinder in a clockwise direction will generate only internal waves propagating to the right.

In a uniformly stratified fluid of infinite extent, the classic 'St Andrew's cross' wave pattern (Mowbray & Rarity 1967) suggests four possible directions of wave radiation. It has been shown experimentally (Gavrilov & Ermanyuk 1997) that in the case of small circular oscillations of a circular cylinder, the four-beam wave pattern degenerates into a two-beam pattern so that for a clockwise motion the energy is radiated only into the first and third quadrants of the Cartesian coordinate system,

with the origin taken at the centre of the cylinder trajectory. A rigorous theoretical consideration of this effect is presented in Hurley & Hood (2001) within the framework of Hurley (1997). This internal-wave pattern has common features with that observed for baroclinic tides. Numerical and experimental studies on baroclinic tides reveal the beam-like structure of the internal wave field with a single beam undergoing reflections between the free surface and the bottom (see e.g. Vlasenko, Stashchuk & Hutter 2005; Garrett & Kunze 2007; Gostiaux & Dauxois 2007).

In the case of 'classic' wave generators undergoing vertical or horizontal oscillations in a uniformly stratified fluid, only a quarter of the total wave power is radiated in a single ray. Such 'classic' generators have been used in the studies on the beam reflection at slopes (see e.g. Peacock & Tabaei 2005). A circular cylinder undergoing the orbital motion may serve as a wave generator concentrating higher energy in a single beam, which is important in studies of nonlinear processes. A detailed review of existing methods of the wave-beam generation as well as the novel technique allowing us to generate a single beam with a remarkably good spatial and temporal monochromaticity are presented in Gostiaux *et al.* (2007).

The experimental results of Gavrilov & Ermanyuk (1997) were obtained by a simple method of colour layering, allowing only a qualitative demonstration of the effect. In the present paper, we re-visit the problem of internal-wave radiation by circular oscillations of a circular cylinder in a uniformly stratified fluid. We focus on the manifestations of nonlinear effects when the radius of the cylinder trajectory increases and compare the effects observed for circular and rectilinear oscillations of the same magnitude. As follows from the above introductory notes, in the case of circular oscillations we may expect strong nonlinear interaction between wave radiation and vorticity generation at the cylinder surface. On one hand, the stirring region around the cylinder should increase the effective size of the oscillatory disturbance; on the other hand, stirring serves as a dissipative mechanism that may essentially decrease the intensity of the radiated waves. In addition, if the typical size of the stirred region, the amplitude of oscillations and the size of the body D are comparable quantities, the time scale of order D^2/ν associated with the diffusion of vorticity may be large compared to the period of oscillations (here ν is the reference kinematic viscosity of a fluid). Under appropriate conditions, this time scale may have relevance to the dynamics of the stirring region and, as a result, to the transient processes of the wave-beam formation.

In the present paper, we also consider the radiation of the second-harmonic wave when the frequency of oscillations is lower than half of the buoyancy frequency. The radiation of the second-harmonic wave has been observed in Mowbray & Rarity (1967). Quantitative measurements of the intensity of perturbations in second- and first-harmonic waves are presented in Sutherland & Linden (2002). However, it is difficult to say *a priori* what would be the ratio between the intensities of second- and first-harmonic waves in the case of circular oscillations, and whether or not the second-harmonic wave pattern would consist of two beams instead of four.

As the main experimental tool we use the synthetic schlieren technique described in Sutherland *et al.* (1999) and Dalziel, Hughes & Sutherland (2000). Some important notes concerning the extension of the technique to the optical disturbances without linearization are presented in Scase & Dalziel (2006). A modification of the synthetic schlieren technique in the case of an axisymmetric internal wave is described in Onu, Flynn & Sutherland (2003) and Flynn, Onu & Sutherland (2003).

The description of the experimental installation and techniques is given in § 2 of the present paper. The results of experiments with internal waves generated by circular

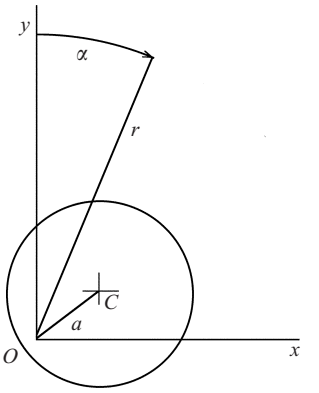

FIGURE 1. Notation.

and rectilinear oscillations of a circular cylinder are described in § 3. A brief summary is presented in § 4.

2. Experimental set-up and procedure

Experiments were carried out in a Perpex test tank of length 160 cm, width 20 cm and height 50 cm. The tank was filled to a depth of 47 cm with a uniformly stratified fluid. The ends of the test tank were equipped with wave absorbers made of perforated flat plates. Uniform stratification was created by the conventional 'double-bucket' method. The linearity of the resulting density profile was checked by a conductivity probe calibrated over the samples of known density. These data were used to evaluate the background buoyancy (Brunt–Väisälä) frequency $N_0 = [-(g/\rho)\mathrm{d}\rho/\mathrm{d}y]^{1/2}$, where g is the acceleration due to gravity, and $\rho(y)$ is the undisturbed density distribution over the vertical coordinate. The value of the background buoyancy frequency in the present experiments was $N_0 = 0.9\,\mathrm{s}^{-1}$.

Internal waves were generated by a circular cylinder of diameter $D = 2$ cm. The cylinder was fixed to a vertical streamlined support and positioned at the centre of the fluid volume. The cross-section of the support was $2 \times 0.2\,\mathrm{cm}^2$. The perturbations induced by the support were negligibly small. Two mechanical gears were used to drive the motion. One gear produced vertical or horizontal sinusoidal oscillations, and the other gear produced circular oscillations. In experiments, the fluid had a free surface. However, owing to the small frequency of oscillations and the small ratio between the diameter of the cylinder and the fluid depth, the presence of a free surface had no detectable effect on the experimental data.

A schematic sketch of notations is shown in figure 1. In the case of circular oscillations, the variation of coordinates of the cylinder centre C with time is described (for clockwise motion) by $x_c = a\sin(\omega t)$ and $y_c = a\cos(\omega t)$, where a is the radius of the cylinder trajectory and ω is the oscillation frequency. Accordingly, the initial coordinates of the cylinder centre at $t = 0$ are $x_c = 0$ and $y_c = a$. The cases of rectilinear horizontal and vertical oscillations correspond to $y_c \equiv 0$, $x_c = -a\cos(\omega t)$ and $x_c \equiv 0$, $y_c = a\cos(\omega t)$, respectively.

The major part of the experimental data obtained with the synthetic schlieren technique (see e.g. Sutherland *et al.* 1999, 2000; Sutherland & Linden 2002) is related to the distribution of the density-gradient disturbances across the main wave beams. In the present paper we are interested in the general structure of wave disturbances

around the cylinder. For representation of results we introduce an additional polar coordinate system $rO\alpha$ (figure 1). To represent the 'zero-frequency' disturbance conveniently, the angular coordinate α is measured in a clockwise direction from the vertical.

A synthetic schlieren system is used for visualization and quantitative measurement of internal waves. The theoretical background and experimental implementation are described in detail in Sutherland *et al.* (1999) and Dalziel *et al.* (2000). Synthetic schlieren is based on the analysis of optical distortions due to internal waves in a continuously stratified fluid. An image of a screen with a contrasting black and white pattern is placed at one side of the test tank and is recorded by a digital camera placed on the other side of the tank. The apparent displacement of the elements of the pattern can be related to the distortions of the density gradient. The linear analysis presented in Sutherland *et al.* (1999) and Dalziel *et al.* (2000) shows that the apparent vertical displacement of an element of the pattern δ_y from its initial position observed through the fluid at rest is directly proportional to the local change in the buoyancy frequency so that $\Delta N^2 = -B\delta_y$. For the set-up used in the present experiments we have $B = 3.34\,\mathrm{s^{-2}\,cm^{-1}}$. The constant B is related to the geometrical parameters and the physical constants of the problem (Sutherland *et al.* 1999). Keeping the notation used in (2.11) of Sutherland *et al.* (1999), the geometrical parameters are the width of the tank $L_t = 20\,\mathrm{cm}$, the distance between the tank and the screen $L_s = 31\,\mathrm{cm}$, and the thickness of the walls of the tank $L_p = 1.45\,\mathrm{cm}$. The camera was placed at distance $L_c = 300\,\mathrm{cm}$ from the test tank. The physical constants include gravity, the indices of refraction of all substances along the path of a light ray from the screen to the camera (i.e. air, water and the material the tank walls are made of), and the rate of change of the index of refraction with the density of solution $\gamma = (\rho_{00}/n_{00}g)(\mathrm{d}n/\mathrm{d}\rho)$. Here, ρ_{00} and n_{00} are the density and the refraction coefficient at a certain (say, zero) concentration of a solute. In the present experiments, the stratification was created using a sugar solution. The corresponding value of γ was evaluated from the data on the optical properties of sugar–water solutions presented in Bronshtein, Gurov & Kuznetsov (1959). For a sugar–water solution we have $\gamma = 2.852 \times 10^{-4}\,\mathrm{s^2\,cm^{-1}}$, an appreciably higher value than $\gamma = 1.878 \times 10^{-4}\,\mathrm{s^2\,cm^{-1}}$ in the case of a salt solution (see Sutherland *et al.* 1999).

In the following section, we use a non-dimensional representation of the buoyancy frequency perturbations in the form $w_y = -\Delta N^2/N_0^2$. According to (2.13) in Sutherland *et al.* (1999), w_y has the physical sense of the derivative of the vertical displacements of fluid particles in internal wave $w(x, y)$ over vertical coordinate y.

For quantitative measurement of displacements δ_y and practical implementation of the synthetic schlieren technique we have used a standard cross-correlation analysis performed with DANTEC Flowmanager software. The possibility of using a cross-correlation technique as a tool for synthetic schlieren data treatment has been already mentioned in Dalziel *et al.* (2000). A contrast pattern of randomly spaced black dots was printed on the white illuminated screen placed behind the test tank. The parameters of the pattern were chosen with regard to recommendations for optimum particle seeding and size presented in Westerweel (1997). A typical image of the screen and the cylinder is shown in figure 2. Videos were taken with a FlowSense M2/E camera having a CCD matrix of size 1600×1186 pixels. The apparent vertical displacements of dots were measured on a grid of interrogation areas. Interrogation areas of 32×32 with a 75 % overlap yielding roughly 29 000 displacement vectors per image were used. Additional calculations were performed with the interrogation areas 16×16 having 50 % overlap. The results obtained with both interrogation grids were

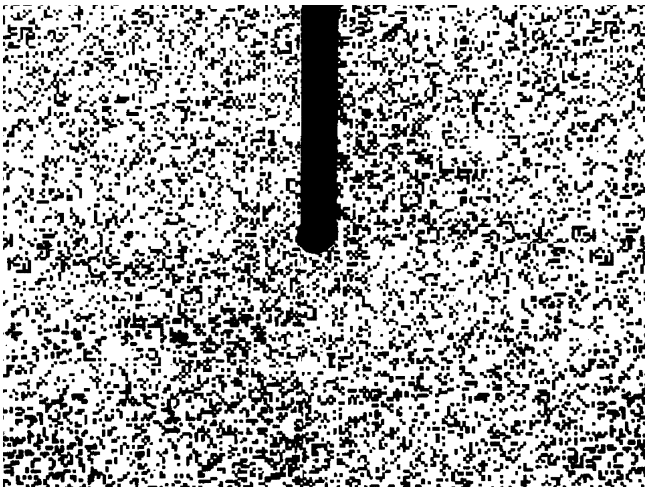

FIGURE 2. View of the cylinder fixed at the vertical support, and a part of the screen. The horizontal size of the support is 2 cm.

found to be in good agreement, although the latter results were characterized by a higher noise level. The information on measuring errors is presented in the Appendix.

3. Results and discussion

Experiments were performed for circular, horizontal and vertical directions of oscillations at $a/D = 0.15, 0.3$ and 0.45 for several values of the non-dimensional oscillation frequency $\Omega = \omega/N$. The characteristic densimetric Stokes number for the present experiments is $\beta = D^2 N_0/\nu = 260$, where ν is the kinematic viscosity at the depth corresponding to the origin of the coordinate system xOy. The results of qualitative visualization reported in Gavrilov & Ermanyuk (1997) have been obtained at a single value of the orbital motion radius $a/D = 0.17$, and $\beta = 840$.

The kinematic viscosity of the sugar solution increases with the concentration of sugar. At a value of $N_0 = 0.9\,\mathrm{s}^{-1}$, the kinematic viscosity of the sugar solution at a depth of 47 cm (near the bottom of the test tank) is twice as high as in the pure water (i.e. at the free surface). However, most of the data presented in this paper refer to the region with a vertical size of 24 cm (i.e. $\pm 6D$ from the origin of the coordinate system). Within this region the kinematic viscosity increases by 25 %. Thus the value of $\beta = 260$ defined by the reference value of ν at the mid-depth of fluid applies to the area of measurements with an accuracy of ± 13 %. Judging from the experimental data obtained in the upper and lower quadrants of the coordinate system xOy, the variation of ν in the measurement zone had practically no influence on the results. The reference data on the properties of the sugar–water solution were taken from Vargaftik (1963) and Bronshtein, Gurov & Kuznetsov (1959).

3.1. *Oscillations at frequency* $0.5 < \Omega < 1$

First, we describe the results obtained in the frequency range $0.5 < \Omega < 1$. In this range, the nonlinear generation of the second harmonic (i.e. waves corresponding to frequency 2Ω) is physically impossible. The effects observed at $0.5 < \Omega < 1$ are illustrated quantitatively by the results obtained at $\Omega = 0.76$. At this frequency, the internal-wave beams forming the 'St Andrew's cross' pattern are inclined at the angle

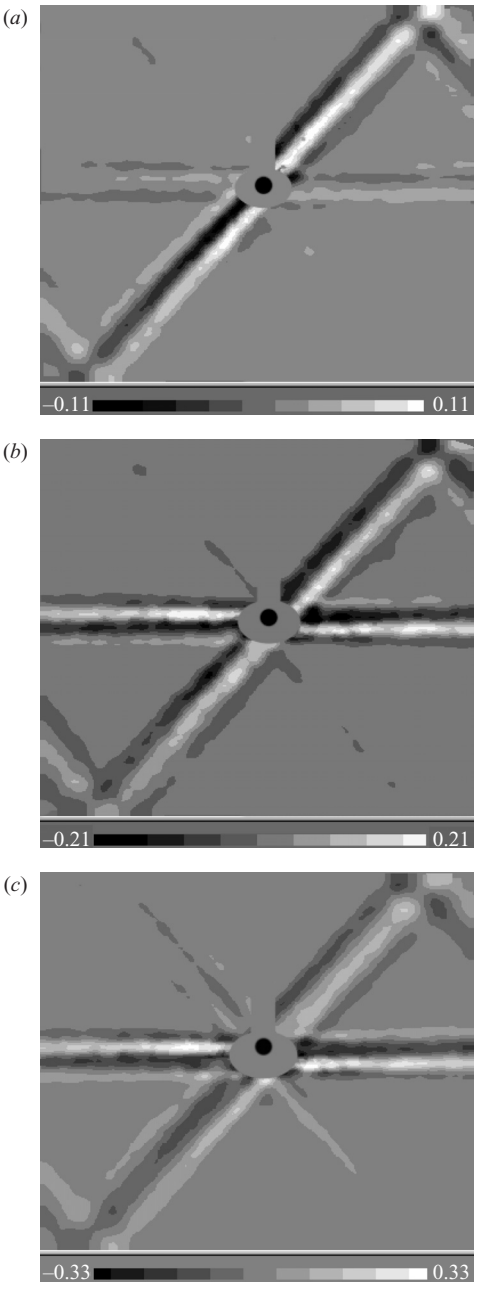

FIGURE 3. Internal wave pattern in the case of circular oscillations. Grey levels show the field of w_y. Cases (*a*), (*b*) and (*c*) correspond to $a/D = 0.15, 0.3$ and 0.45. For all images $\Omega = 0.76$, $\tau = 20$. The region of high density-gradient perturbations in the vicinity of the cylinder and the region occupied by the cylinder support are filtered out.

$\theta = 41^\circ$ to the vertical in accordance with the dispersion relation:

$$\theta = \arccos \Omega. \tag{3.1}$$

Typical synthetic schlieren images of internal waves generated by orbital clockwise motion and horizontal oscillations of a circular cylinder are shown in figures 3 and 4,

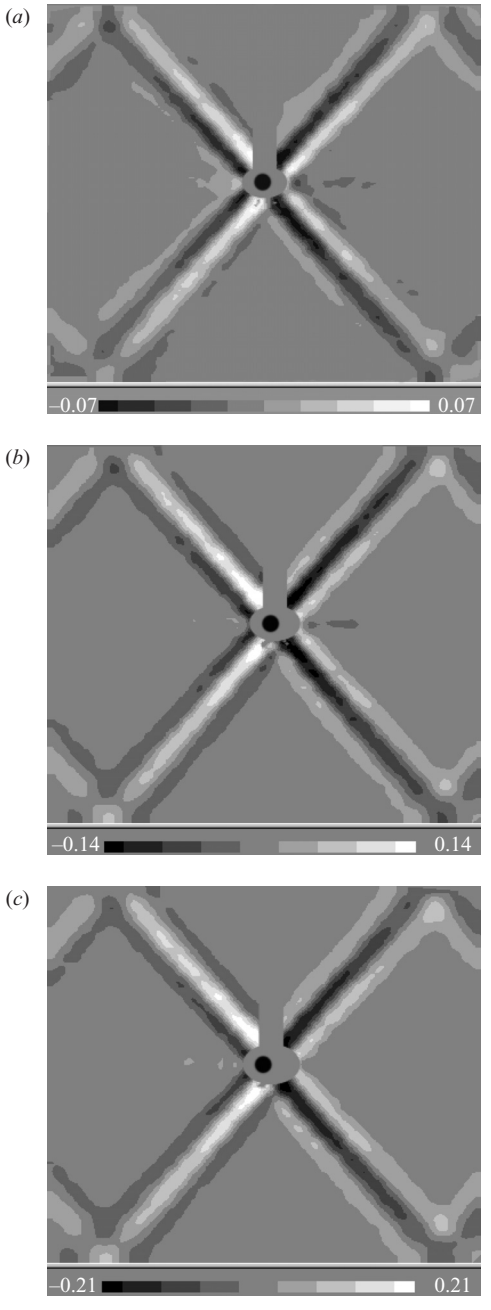

FIGURE 4. Internal wave pattern in the case of horizontal oscillations. Other details are the same as in figure 3.

respectively. The grey levels indicate the field of w_y. Cases (*a*), (*b*) and (*c*) in figures 3 and 4 correspond to $a/D = 0.15, 0.3$ and 0.45. All the images are taken at $\tau = 20$, where non-dimensional time is defined as $\tau = t/T$, with $T = 2\pi/\omega$. The motion starts at $\tau = 0$. The images shown in figure 3 correspond to the phase of motion when the cylinder centre passes the upper point of the trajectory ($x_c = 0$, $y_c = a$). For the images

shown in figure 4, the phase of horizontal oscillations corresponds to $x_c = -a$. The patterns shown in figures 3 and 4 have different symmetry properties. In the case of circular oscillations, we observe symmetry with respect to rotation by 180°, and in the case of horizontal oscillations, the pattern has mirror symmetry with respect to the horizontal plane $y = 0$.

For circular oscillations we can see that the internal-wave pattern at the lowest experimental value of the orbital-motion radius $a/D = 0.15$ is in good qualitative agreement with the predictions of the linear theory (see figure 3*a*). The wave motion is concentrated within beams passing through the first and third quadrants of the Cartesian coordinate system, with a weak density-gradient disturbance in the horizontal stripe extending in the directions $\alpha = \pm\pi/2$ corresponding to $\Omega = 0$ by virtue of (3.1). As the radius of the orbital motion increases (see figure 3*b*, *c*), the density-gradient disturbance at zero frequency increases markedly so that for $a/D = 0.45$, the maximum magnitudes of w_y in the horizontal stripe are higher than the maximum magnitudes of w_y observed in the main wave beams. Also, we can see that the secondary wave radiation into the second and fourth quadrants markedly increases with a/D.

For horizontal oscillations (see figure 4), the waves in the 'St Andrew's cross' beams represent the dominant feature of the observed internal-wave pattern for all studied values of a/D. The density-gradient 'zero-frequency' disturbance remains relatively small. The presence of this disturbance in the case of rectilinear oscillations has been mentioned, for example, in Dalziel (2000) and Sutherland & Linden (2002). Since the density stratification prohibits the formation of the circulating sells observed in the case of rectilinear oscillation of a cylinder in a homogeneous fluid, the zero-frequency disturbance may be attributed to diffusive mixing near the sloping boundaries of the cylinder (Phillips 1970; Wunsch 1970; Linden & Weber 1977; Baidulov & Chashechkin 1993, Baidulov & Chashechkin 1996).

In the case of orbital motion, the development of the zero-frequency disturbance seems to be associated mainly with the mass-transfer nearly horizontal currents induced by the moving cylinder. When the cylinder sweeps the upper part of the trajectory in the clockwise direction, it acts as a piston moving from left to right, forcing the corresponding horizontal motion of the stratified fluid. In the lower part of the trajectory, the cylinder acts similarly as a piston moving from right to left. Since the amplitude of the motion is finite, such forcing results in two counter-directed currents (from left to right at $y > 0$ and vice versa at $y < 0$). This explanation appeals to the effect akin to blocking, and such a mechanism seems to be effective at $\Omega < 1$ (including vanishingly small Ω) when gravity dominates over inertia.

For better quantitative comparison between the effects observed for circular and horizontal oscillations, we consider the distributions of w_y along the angular coordinate α. The distributions were sampled with the increment $\Delta\alpha = 1°$. The random measurement noise was filtered out by the standard procedure of Gaussian smoothing with the bandwidth 3°. We take distribution $w_y(\alpha)$ at distance $6D$ from the origin of the coordinate system xOy as a representative one. At this distance, the wave motions in the inclined beams and the zero-frequency perturbation in the horizontal stripe are well separated in space for the values of a/D studied in the present experiments. At the same time we can trace the variations of the shapes of wave envelopes in the cases of circular and horizontal oscillations. The distributions $w_y(\alpha)$ are shown in figures 5 and 6 for circular and horizontal oscillations, respectively, where cases (*a*), (*b*) and (*c*) correspond to $a/D = 0.15$, 0.3 and 0.45. Left- and right-hand parts in figures 5 and 6 correspond to periods 10 and 20 after the start of

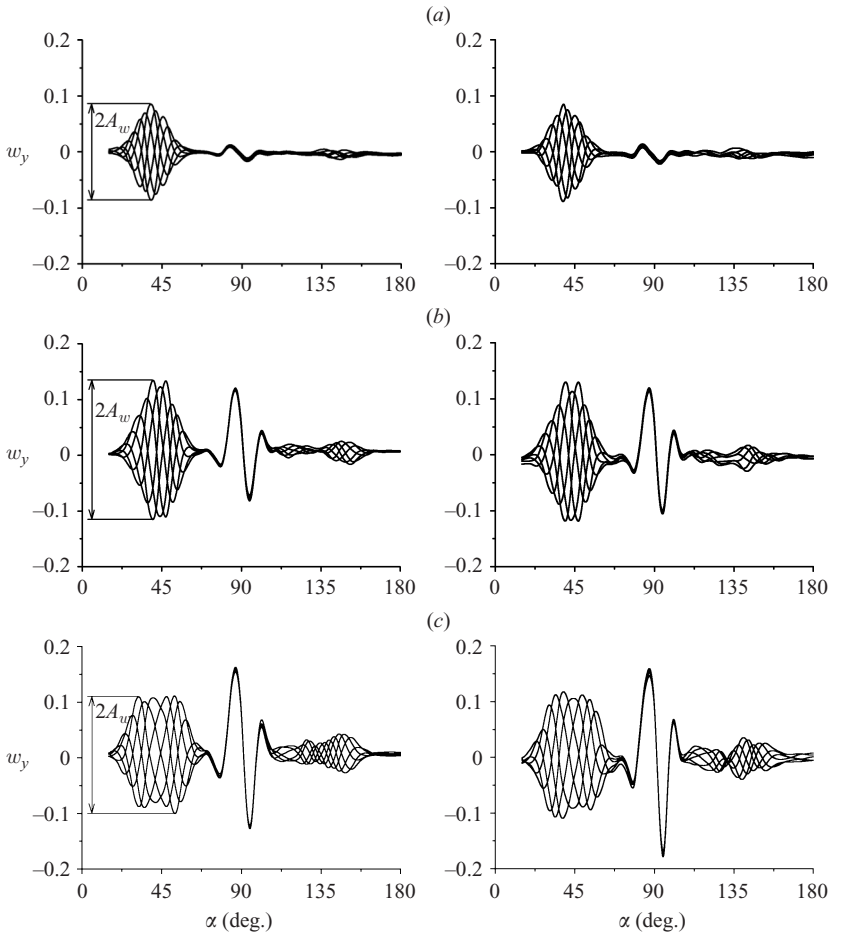

FIGURE 5. Profiles of $w_y(\alpha)$ in the case of circular oscillations for periods number 10 (left-hand side) and 20 (right-hand side) after the start of the motion. All profiles are taken at distance $6D$ from the origin of the coordinate system shown in figure 1, $\Omega = 0.76$. The phase increment between the successive profiles is $\pi/3$. Cases (*a*), (*b*) and (*c*) correspond to $a/D = 0.15, 0.3$ and 0.45. The envelope magnitude $2A_w$ is defined in the left-hand profiles.

the motion. Successive profiles $w_y(\alpha)$ are shown with the phase increment of $\pi/3$ (6 profiles per period). The comparison of profiles taken 10 and 20 periods after the start of the motion shows that the magnitude of the envelopes $2A_w$ (defined in the left-hand parts of figures 5 and 6) is a sufficiently stable quantity that it can be used as a parameter characterizing the intensity of wave motions in the main wave beams. The transient effects associated with the formation of wave beams are discussed later. To characterize at first approximation the linear/nonlinear properties of waves in the main beams we introduce $\eta_w = A_w/(a/D)$, which can be interpreted as a response/excitation ratio. The mean values of η_w at $a/D = 0.15, 0.3$ and 0.45 are presented in table 1 for circular, horizontal and vertical oscillations. The mean values were determined from the data obtained for periods 10 and 20 for four beams in the cases of horizontal and vertical oscillations and for two beams in the case of circular oscillations. The typical scatter of data was about $\pm 5\,\%$ of the mean values. We can see that at $a/D = 0.15$ the data are in good agreement with a linear scenario:

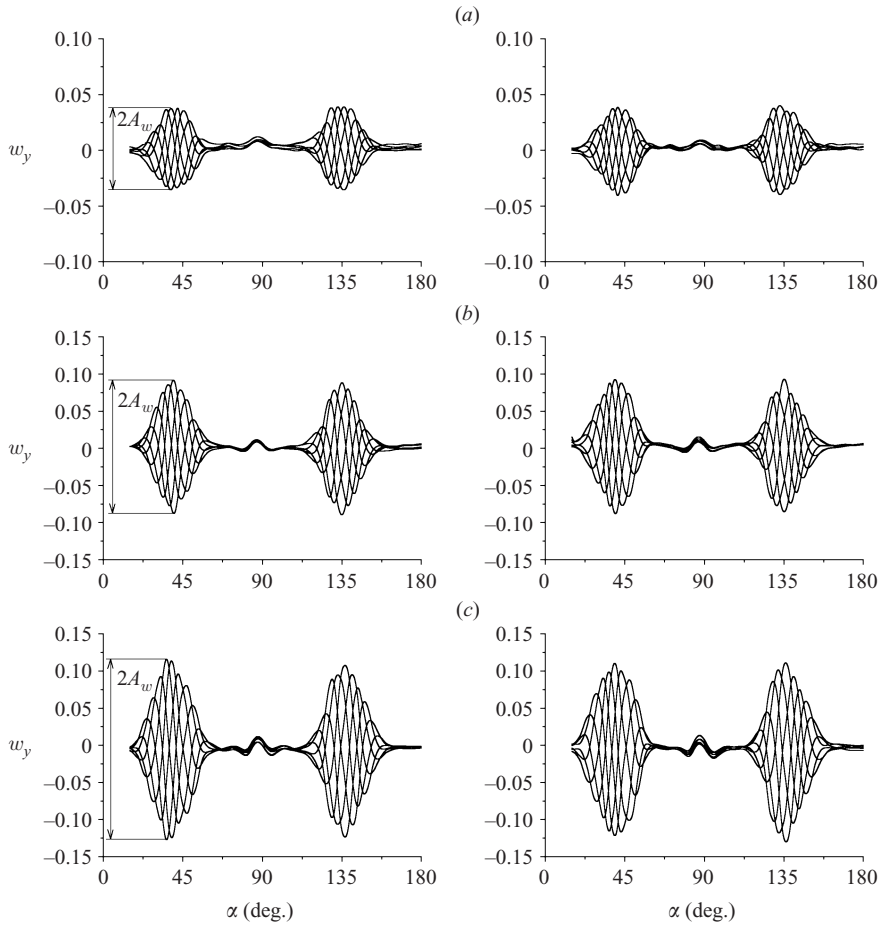

FIGURE 6. Profiles of $w_y(\alpha)$ in the case of horizontal oscillations for periods 10 (left-hand side) and 20 (right-hand side) after the start of the motion. Legend is the same as in figure 5.

	Type of oscillations					
	Circular		Horizontal		Vertical	
a/D	η_w	η_w^{rms}	η_w	η_w^{rms}	η_w	η_w^{rms}
0.15	0.58	0.59	0.28	0.26	0.27	0.25
0.3	0.42	0.42	0.3	0.29	0.28	0.26
0.45	0.25	0.26	0.26	0.26	0.26	0.23

TABLE 1. The values of η_w and η_w^{rms} for different types and amplitudes of oscillations.

η_w in the case of circular oscillations is twice the value of η_w measured for horizontal and vertical oscillations to within the experimental accuracy. However, for higher values of a/D we observe strong manifestations of nonlinearity in the case of circular oscillations.

To illustrate the effects of nonlinearity we have estimated the across-beam amplitudes by using a procedure similar to that described in Sutherland & Linden

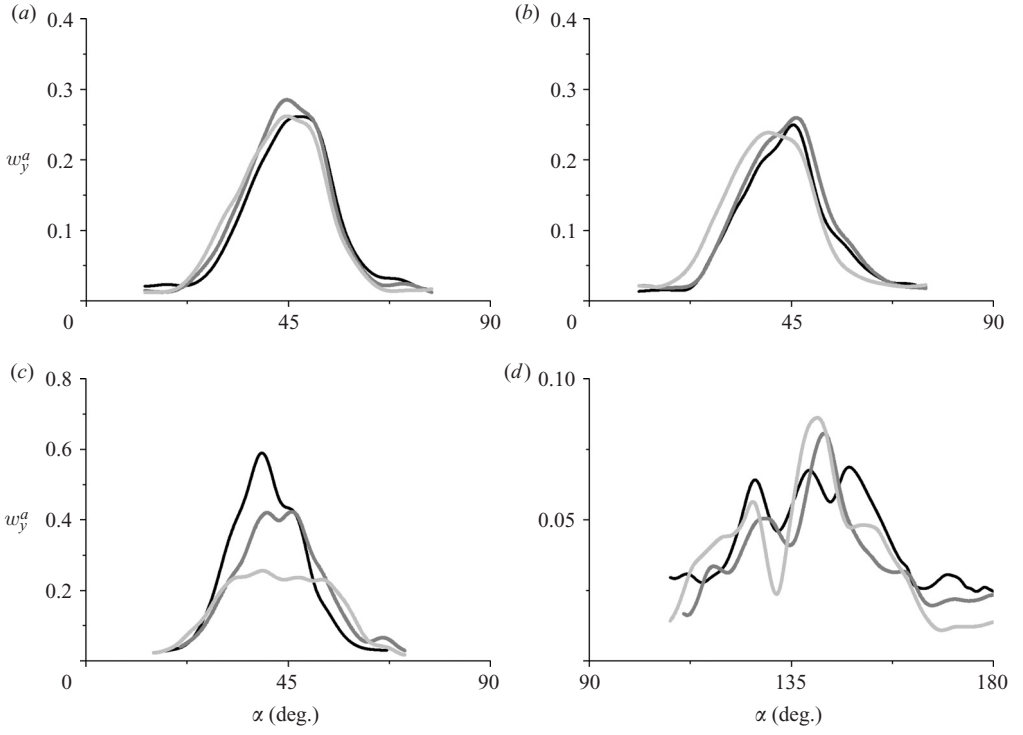

FIGURE 7. Envelopes of internal wave beams in the cases of (*a*) horizontal, (*b*) vertical, and (*c*), (*d*) circular oscillations. Cases (*a*) – (*c*) correspond to the beams passing through the first quadrant of the coordinate system xOy; case (*d*) corresponds to the secondary wave beam in the fourth quadrant. The envelopes are calculated for period 20 after the start-up of the motion. All envelopes correspond to distance $6D$ from the point O, and $\Omega = 0.76$. Black, grey and light grey lines correspond to $a/D = 0.15, 0.3$ and 0.45, respectively. Note the difference of the vertical scales in the figures.

(2002) (a typical resulting distribution of across-beam amplitude is shown in their figure 10). The envelopes were obtained by calculating the root-mean-square (r.m.s.) average of time series of w_y and multiplying them by $2^{1/2}$ to obtain the distribution of amplitudes of fluctuations of w_y^a over α. The r.m.s. values were calculated using 12 samples of w_y taken at the twentieth period of oscillation. Further, we normalize the ordinates of the envelopes by a/D. The resulting envelopes $W_y^a = w_y^a/(a/D)$ are shown in figure 7, where cases (*a*), (*b*) and (*c*) correspond to horizontal, vertical and circular oscillations, respectively. The maximum values of the envelopes $\eta_w^{rms} = \max(W_y^a(\alpha))$ are given in table 1 together with the values of η_w. We can see that the two methods of evaluation yield very similar results.

In the case of vertical and horizontal oscillations, the width of the envelopes increases with a/D, as could be expected. At the same time, η_w^{rms} depends only weakly on a/D. The experiments with vertical and horizontal oscillations were performed at the same value of Ω. The maximum of $W_y^a(\alpha)$ in the case of vertical oscillations with $a/D = 0.45$ appears to be shifted toward smaller α as compared to the case of horizontal oscillations (compare light grey lines in figure 7*a* and 7*b*).

In the case of circular oscillations (figure 7*c*), we observe strong qualitative and quantitative variation of the wave envelopes with a/D. At $a/D = 0.15$, the wave envelope in the main beam is roughly bell-shaped, similar to the envelopes observed

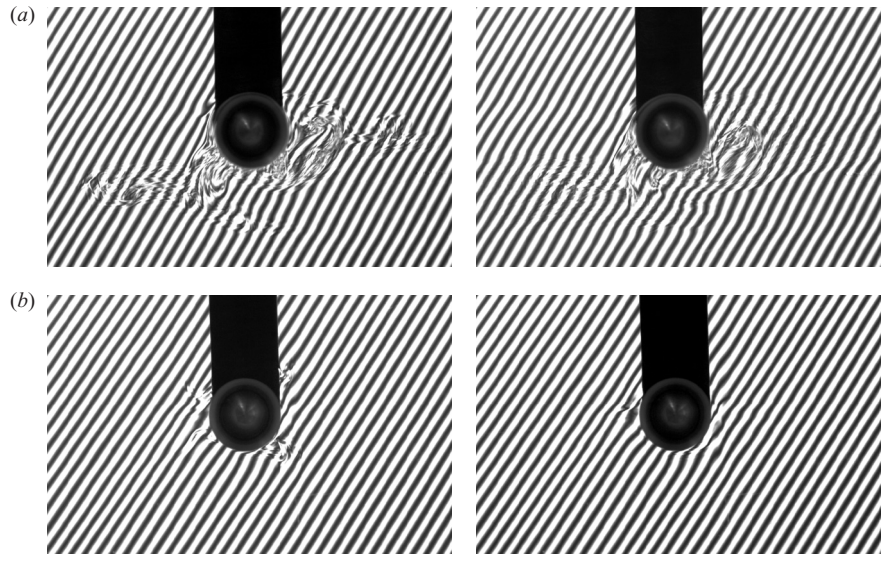

FIGURE 8. Flow structure in the near region of the oscillating cylinder for (*a*) circular and (*b*) horizontal oscillations. Left- and right-hand images correspond to $\tau = 2$ and 10 in (*a*) and $\tau = 1.75$ and 9.75 in (*b*); $a/D = 0.45$, $\Omega = 0.76$. The cylinder centre is located at $x_c = 0$, $y_c = a$ in (*a*) and $x_c = 0$, $y_c = 0$ in (*b*).

for the rectilinear oscillations (figure 7*a*, *b*). As a/D increases, the envelope tends to be first bi-modal ($a/D = 0.3$) and then plateau-shaped ($a/D = 0.45$).

The shape of the envelopes in the secondary wave beam at low a/D is obscured by the instrumental noise (figure 7*d*). However, at $a/D = 0.45$, the signal-to-noise ratio is sufficiently large and the shape of the envelope is well defined. We observe a local minimum of the envelope at the angle $\alpha \approx 135^\circ$. This is in agreement with the profiles shown in figure 5(*c*) and with the data presented at the spatiotemporal images discussed further in the text.

As a/D increases, the intensity of the waves radiated in the main beams in the case of circular oscillations drastically decreases compared to the values that might be expected in the case of a linear process. For example, at $a/D = 0.45$, the values of η_w and η_w^{rms} measured for circular oscillations practically coincide with those measured for vertical and horizontal oscillations (see table 1). We believe that the decrease of η_w and η_w^{rms} with increase of a/D in the case of circular oscillations is associated with the additional energy dissipation due to stirring in the near region of the cylinder, and due to generation of nearly horizontal currents.

The patterns of stirring in the near region of the cylinder are shown in figure 8(*a*) and 8(*b*) for circular and horizontal oscillations, respectively. The visualization was performed by capturing the image of an illuminated pattern of black and white stripes through the bulk of the fluid. This simple method effectively reveals the qualitative features of the flow structure (Ermanyuk & Gavrilov 2007). The images are taken at $\tau = 2$ and 10 in the case of orbital motion and at $\tau = 1.75$ and 9.75 in the case of horizontal oscillations at $a/D = 0.45$ and $\Omega = 0.76$. We can see that the size of the stirred region in the case of circular oscillations far exceeds the size of the stirred region in the case of horizontal oscillations. Periodic vortex generation in the stirred region owing to the orbital motion of the cylinder is believed to be the

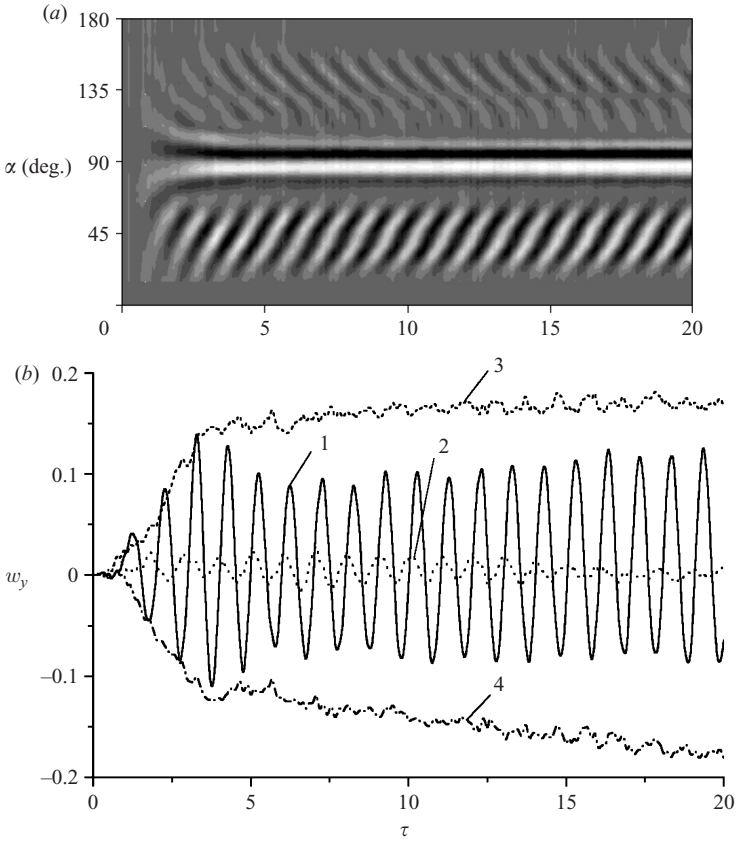

FIGURE 9. (*a*) Spatiotemporal image $w_y(\alpha, \tau)$ and (*b*) representative time-series $w_y(\tau)$ at different values of α in the case of circular oscillations at $a/D = 0.45$. The data correspond to distance $r = 6D$, $\Omega = 0.76$. Lines 1 – 4 in (*b*) correspond to $\alpha = 45°, 135°, 87°, 95°$, respectively.

main excitation mechanism for secondary internal-wave radiation into the second and fourth quadrants.

The diagrams of flow regimes for vertical and horizontal oscillations of a circular cylinder at $0.15 < a/D < 2$ and $0.16 < \Omega < 6$ have been obtained in Xu *et al.* (1997). The range of experimental parameters covered in the present study corresponds to the regimes identified in Xu *et al.* (1997) as 'weakly detached flow' and the onset of 'localized mixing', which is in agreement with our data for rectilinear oscillations.

The time evolutions of $w_y(\alpha, \tau)$ for circular and horizontal oscillations at distance $6D$ from the origin are shown in figures 9(*a*) and 10(*a*) in the form of spatiotemporal images for $a/D = 0.45$, $\Omega = 0.76$ (a similar technique has been used in Sutherland & Linden 2002). The first 20 periods after the start are shown. The profiles $w_y(\alpha)$ were sampled at the rate of 12 profiles per period. Figures 9(*b*) and 10(*b*) show the cross-sections of the spatiotemporal images along the time axis for a set of representative angles. In the case of circular oscillations, the representative values of α are taken as 45° and 135°, approximately corresponding to the middle of the main beam and to the local minimum of the envelope in the secondary wave beam, and 87° and 95° corresponding to maximum positive and negative values of w_y in the horizontal stripe. In the case of horizontal oscillations, the representative values of α are taken as 42° and 138°, approximately corresponding to the maximums of the envelope,

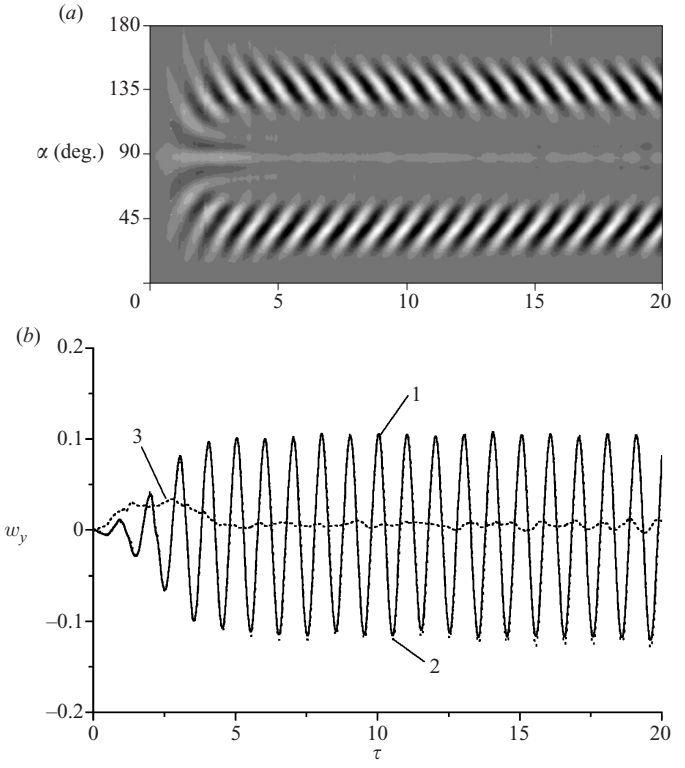

FIGURE 10. (*a*) Spatiotemporal image $w_y(\alpha, \tau)$ and (*b*) representative time series $w_y(\tau)$ at different values of α in the case of horizontal oscillations at $a/D = 0.45$. The data correspond to distance $r = 6D$, $\Omega = 0.76$. Lines 1–3 in (*b*) correspond to $\alpha = 42°, 138°, 90°$, respectively. Owing to mirror symmetry, lines 1 and 2 practically coincide.

and 90° corresponding to maximum disturbance at 'zero' frequency. It can be seen that the transient processes in the case of circular and horizontal oscillations are essentially different. In the case of horizontal oscillations the oscillation magnitude (lines 1 and 2 in figure 10*b*) in the wave beams tend to approach the steady-state value monotonically, whereas in the case of circular oscillations it tends first to overshoot (line 1 in figure 9*b*) the steady-state value. Note that because of mirror symmetry, lines 1 and 2 in figure 10(*b*) practically coincide. The oscillatory process represented by lines 1 and 2 in figure 10(*b*) reaches the steady state at τ between 7 and 10. The duration of the transient process is in good agreement with earlier experimental data presented in a preliminary paper by Ermanyuk & Gavrilov (2005) for a vertically oscillating cylinder. In Ermanyuk & Gavrilov (2005), the fields of w_y were sampled at a fixed phase of vertical oscillations of a circular cylinder (i.e. at the rate of one image per period of oscillations) and the time scale of transients was evaluated from the period-to-period evolution of an appropriately formulated correlation coefficient for distributions $w_y(\alpha)$ taken at a set of distances from the body. The data obtained in Ermanyuk & Gavrilov (2005) at $a/D = 0.3$, $\Omega = 0.7$, $D = 2\,\mathrm{cm}$ and $N = 1.05\,\mathrm{s}^{-1}$ suggest the time scale of the transient processes $\tau \approx 6$ for $r = 4D$.

Comparing line 1 in figure 9(*b*) with line 1 in figure 10(*b*) at $\tau > 10$ (i.e. when the steady-state oscillations are reached), we observe a higher cycle-to-cycle amplitude variation in the former case. We believe that the fluctuations of the amplitude in the

case of orbital motion are related to cycle-to-cycle variability of the vortex generation in the region of intense stirring around the cylinder.

Note that the transient process observed with the novel internal-wave beam generator described in Gostiaux *et al.* (2007) reminds us of a sudden 'switch-on' of sine oscillations (see figure 6*a* therein) with vanishingly short transients. In the present study, in the main beams we observe transient processes evolving at a time scale of several periods. These experimental facts emphasize the importance of further investigations into the relation between the dynamics of transients and the particular mechanisms of internal-wave excitation.

The time evolution of the secondary wave beam in the case of circular oscillations has some interesting properties. A closer inspection of the upper part of figure 9(*a*) shows that after approximately 8 periods of oscillation the secondary wave beam starts to separate into two parallel beams so that the direction $\alpha = 135^\circ$ approximately correspond to the minimum of the wave intensity: at $15 < \tau < 20$ the variation of the grey level along $\alpha = 135^\circ$ is small, while above and below this line the variation of the grey level with τ is much more pronounced. Small wave intensity at $\alpha = 135^\circ$, i.e. approximately in the middle of the secondary wave beam, suggests that the wave-making zones are located close to the upper and the lower points of the region swept by the cylinder. Line 2 in figure 9(*b*) shows that the intensity of fluctuations of w_y at $\alpha = 135^\circ$ reaches a maximum at $\tau \simeq 8$ and gradually decays at $8 < \tau < 20$. The time scale of the secondary wave beam evolution may be associated with the dynamics and evolution of the stirred region around the cylinder. The time scale of the vorticity diffusion is known to be of order l^2/ν, where l is the typical length scale of a vortex structure. The time scales $8T$ and $20T$ suggest l between $0.5D$ and $0.8D$.

In the horizontal stripe, maximum positive and negative disturbances (lines 3 and 4 in figure 9*b*) in the case of circular oscillations do not reach saturated values within the first 20 periods of oscillations. Since there is a continuous horizontal pumping of fluid owing to orbital motion of the cylinder, there are reasons to believe that the steady state in the horizontal stripe cannot be reached. The orbital motion ultimately leads to formation of sharp horizontal density interfaces. In contrast, in the case of horizontal oscillations the 'zero-frequency' disturbance tends not to increase during the span of time studied (line 3 in figure 10*b*). Additional data on the processes in the horizontal stripe at $0 < \Omega < 0.5$ and $\Omega > 1$ are presented in subsequent subsections.

To visualize the horizontal currents induced by circular oscillations, vertical tracers in the otherwise quiescent fluid were produced by dropping small grains of sugar covered with dye. The evolution of the tracer profiles owing to horizontal currents after the start of the orbital motion was video recorded. The typical shape of the tracers is illustrated in figure 11(*a*) for $\Omega = 0.76$, $a/D = 0.45$, $\tau = 5$. Figure 11(*b*) shows the time evolution of the normalized horizontal displacements of points A and B defined in figure 11(*a*). The normalized displacements are defined as $\Delta\xi_A = (x_A - x_0)/D$ and $\Delta\xi_B = (x_B - x_0)/D$, where x_0 is the initial horizontal coordinate of a tracer line in the quiescent fluid. We can see that for a fixed τ we have $|\Delta\xi_A| < |\Delta\xi_B|$, i.e. the magnitude of a displacement directed toward the cylinder is higher than the magnitude of the outward-directed displacement. The typical vertical size of the current directed toward the cylinder is smaller than that of the outward-directed current so that the mass conservation for the flow across the vertical line drawn at the initial position of the tracer is fulfilled. We should keep in mind that the whole wave and current pattern in the case of circular oscillations has a symmetry with respect to rotation by 180° about point O. At a fixed time instance, the displacements decay with distance while the vertical size of the current involved in the quasi-horizontal motion increases

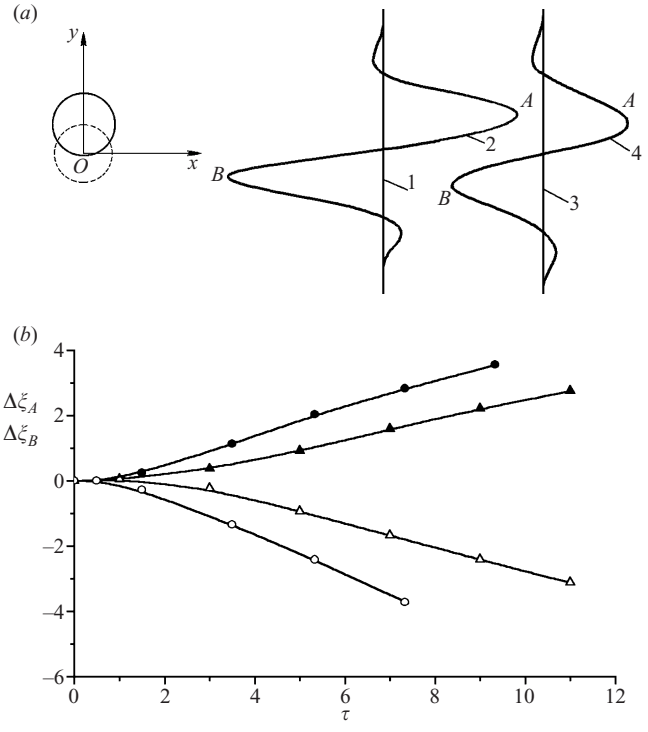

FIGURE 11. Horizontal currents induced by clockwise circular oscillations of the cylinder. Experimental conditions: $\Omega = 0.76$, $a/D = 0.45$. (*a*) Sketch of the tracer distortions. Lines 1 and 3 corresponding to $\tau = 0$ are located at distances $5D$ and $7.5D$ from the point O. Lines 2, 4 correspond to $\tau = 5$. The dashed line shows the circular orbit of the cylinder centre. (*b*) Normalized horizontal displacements of points A (solid symbols) and B (open symbols) *vs.* non-dimensional time. Circles and triangles refer to the tracers initially located at distances $5D$ and $7.5D$, respectively.

with distance, as is apparent from the data obtained at $x_0 = 5D$ and $x_0 = 7.5D$ (compare lines 2 and 4 in figure 11*a*). The data shown in figure 11(*b*) suggest that the horizontal displacements increase with time indefinitely, while the velocity of the nearly horizontal currents at a given distance from the cylinder seems to approach a saturated value.

3.2. *Oscillation at frequency* $0 < \Omega < 0.5$

It is well-known (see Mowbray & Rarity 1967) that a cylinder oscillating at frequency $0 < \Omega < 0.5$ can generate not only the waves at fundamental frequency Ω, but also the waves corresponding to frequency 2Ω. This nonlinear excitation mechanism has been studied in more detail in Sutherland & Linden (2002), where we can find quantitative data on the generation of internal waves at frequency 2Ω by vertical oscillations of an elliptic cylinder. The typical wave patterns observed in the case of circular and horizontal oscillations in our experiments are shown in figures 12(*a*) and 12(*b*) for $a/D = 0.6$, $\Omega = 0.38$, $\tau = 10$. It can be seen that in the case of clockwise orbital motion of the cylinder, internal waves of frequency Ω and 2Ω are primarily radiated into the first and third quadrants of the coordinate system xOy. In the case of horizontal oscillations, the pattern has mirror symmetry with respect to the plane $y = 0$. The corresponding spatiotemporal images $w_y(\alpha, \tau)$ obtained at $r = 10D$ for the first 10

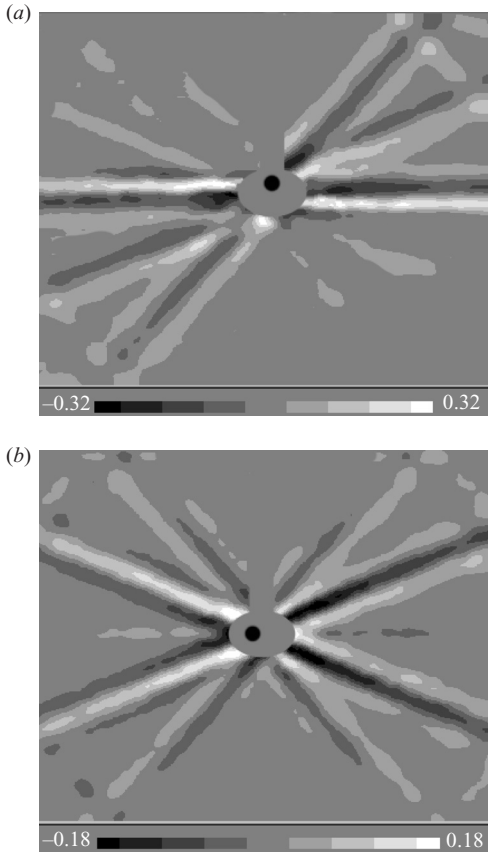

FIGURE 12. Internal wave patterns in the cases of (*a*) circular and (*b*) horizontal oscillations at $a/D = 0.6$, $\Omega = 0.38$, $\tau = 10$. Grey levels show the field of w_y.

periods of oscillations are shown in figures 13(*a*) and 14(*a*). The main trends seen in these figures for circular and horizontal oscillations correspond to those observed in figures 9(*a*) and 10(*a*).

It is interesting to compare the intensities of oscillations of w_y in the beams corresponding to fundamental and doubled frequencies in the cases of circular and horizontal oscillations. In figures 13(*b*) and 14(*b*), we can see the cross-sections of the spatiotemporal images along the time axis for a set of representative angles. The representative values of α are taken as $\alpha = 41^\circ$ and 68°, approximately corresponding to the middles of the beams radiated at $2\Omega = 0.76$ and $\Omega = 0.38$. In the case of circular oscillations, the maximum oscillation amplitudes of w_y in the beam radiated at frequency 2Ω (line 2 in figure 13*b*) are only about 15 % smaller than those corresponding to the beam radiated at frequency Ω (line 1 in figure 13*b*). In the case of horizontal oscillations, the oscillation amplitudes of w_y corresponding to frequency 2Ω are approximately 3 times smaller than those corresponding to frequency Ω (compare lines 1 and 2 in figure 14*b*). The cross-comparison of figures 13 and 14 emphasizes strongly the nonlinear character of wave generation in the case of circular oscillations. The data shown in figures 13 and 14 correspond to the distance $10D$ from the origin of the coordinate system. At this distance there is still some interaction between the beams corresponding to frequencies Ω and 2Ω. In addition to the

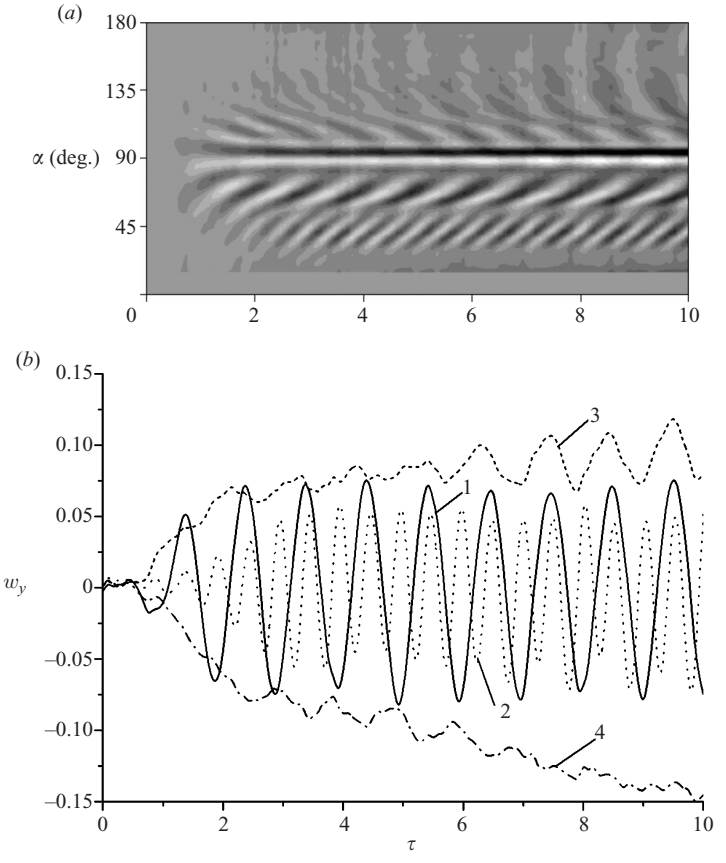

FIGURE 13. (*a*) Spatiotemporal image $w_y(\alpha, \tau)$ and (*b*) representative time-series $w_y(\tau)$ at different values of α in the case of circular oscillations. The data correspond to distance $r = 10D$. Experimental conditions are the same as in figure 12. Lines 1–4 in (*b*) correspond to $\alpha = 68°, 41°, 87°$, and $95°$, respectively.

dominant frequency component corresponding to 2Ω, the fluctuations of w_y at $\alpha = 41°$ (lines 2 in figures 13*b* and 14*b*) contain the component corresponding to frequency Ω.

The development of the perturbations in the horizontal stripe is illustrated by the time series $w_y(\tau)$ taken at $\alpha = 87°$ and $95°$ in the case of circular oscillations (lines 3 and 4 in figure 13*b*), and $\alpha = 90°$ in the case of horizontal oscillations (line 3 in figure 14*b*). Additional experiments have been performed at lower oscillations frequencies ($\Omega \approx 0.2$). The trends observed for the perturbations in the horizontal stripe in the case $0 < \Omega < 0.5$ are, by and large, similar to those observed in the case $0.5 < \Omega < 1$ (compare figures 8, 9 and 13, 14).

3.3. *Oscillation at frequency* $\Omega > 1$

In § 3.1, we have mentioned that the sweeping orbital motion of the cylinder should lead to the piston-type excitation of the counter-directed nearly horizontal currents when the buoyancy effects dominate over inertia and the amplitude of the circular oscillation is finite. The most important feature of such a forcing is that it creates currents having non-zero angular momentum with respect to point O, the origin of the coordinate system shown in figure 1.

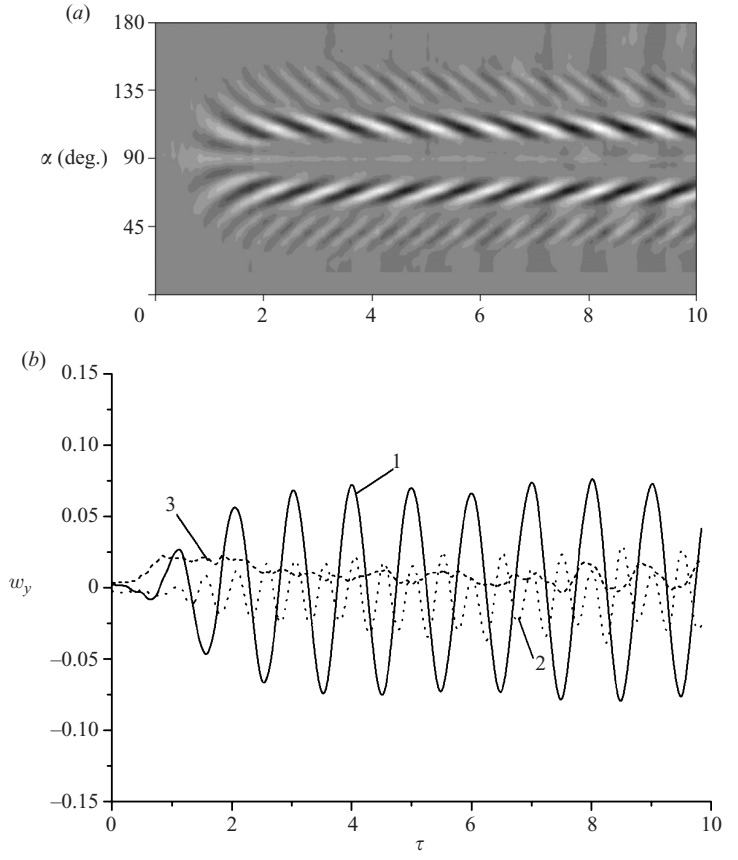

FIGURE 14. (*a*) Spatiotemporal image $w_y(\alpha, \tau)$ and (*b*) representative time-series $w_y(\tau)$ at different values of α in the case of circular oscillations. The data correspond to distance $r = 10D$. Experimental conditions are the same as in figure 12. Lines 1–3 in (*b*) correspond to $\alpha = 68°, 41°, 90°$, respectively.

In the viscous case we can expect that the cylinder undergoing the orbital motion experiences the viscous drag force which produce a non-zero time-averaged moment with respect to the point O. Correspondingly, there must be a current of fluid with a non-zero time-averaged angular momentum with respect to O. In the case of a homogeneous viscous fluid, such a current is represented by a steady circulation around the cylinder (Longuet-Higgins 1970; Riley 1971). Since the presence of the vertical density gradient suppresses the vertical fluid motions, in a uniformly stratified viscous fluid we observe nearly horizontal currents having the non-zero time-average angular momentum with respect to O. This mechanism appeals to the global balance of the angular momentum in a viscous uniformly stratified fluid and applies regardless to the value of Ω. Thus, in the case of circular oscillations, we may expect the presence of horizontal currents not only at $\Omega < 1$, but also at $\Omega > 1$ when inertia dominates over gravity in the near field of the cylinder. By contrast, in the case of rectilinear oscillations, the time-average angular momentum must be zero and we cannot expect large perturbations at 'zero' frequency.

The field of w_y generated by the orbital clockwise motion of a circular cylinder at $\Omega = 1.4$ and $a/D = 0.3$ is shown in figure 15. The image corresponds to the

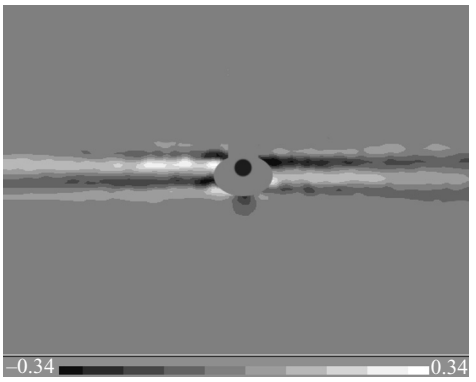

FIGURE 15. The 'zero-frequency' disturbance generated by circular oscillations at $\Omega = 1.4$, $a/D = 0.3$, $\tau = 12$. The cylinder centre is located at $x_c = 0$, $y_c = a$. Grey levels indicate the field of w_y.

non-dimensional time $\tau = 12$, the cylinder centre is located in the point $x_c = 0$, $y_c = a$. For greater insight into the dynamics of the processes in the horizontal stripe at $\Omega > 1$, a series of experiments has been performed for circular, horizontal and vertical oscillations. The results for the fixed amplitude $a/D = 0.3$ and frequency varying in the range $1.1 < \Omega < 2.6$ are shown in figure 16 in the form of the distributions $w_y(\alpha)$ taken at $\tau = 12$. The distributions were taken at the distance $6D$ from the origin O of the coordinate system shown in figure 1, cases (a), (b) and (c) in figure 16 correspond to circular, horizontal and vertical oscillations, respectively. We can see that at fixed a/D and τ the magnitude of the perturbations generated by circular oscillations in the horizontal stripe markedly increases with frequency (figure 16a). The trend toward increase of the magnitude of perturbations with frequency seems to be present in the data for vertical and horizontal oscillations (figure 16b, c). However, in the latter cases, the magnitude of perturbations is smaller by an order of magnitude than in the former one, and the general trends are somewhat obscured by the instrumental noise. It is worth mentioning qualitative similarity between the shapes of profiles of $w_y(\alpha)$ for α around 90° measured at $\Omega > 1$ (figures 16a, b) and at $\Omega < 1$ (figures 5b and 6b) for circular and horizontal oscillations. The same is true for vertical oscillations. In general, the data presented in figure 16 are consistent with the discussion of the angular momentum balance presented in the beginning of this subsection.

The nearly horizontal currents induced by the clockwise circular oscillations at $\Omega > 1$ have been visualized by observing the distortion of vertical tracers. The typical observed shape of the tracer is illustrated in figure 17(a) for $\Omega = 1.17$, $a/D = 0.45$, $\tau = 20$. It can be seen that the pattern is qualitatively similar to that depicted in figure 11(a). However, as the frequency of the orbital motion increases, the stirring and mixing of fluid in the vicinity of the cylinder also increases. Since the mixed region collapses owing to gravity, the continuous production of the mixed fluid in the near region of the cylinder leads to the continuous increase of the horizontal size of the mixed region, and, as result, to the formation of horizontal currents directed away from the cylinder in the vicinity of $y = 0$. To maintain the mass conservation, the flow away from the cylinder should be balanced by the inflows of unmixed fluid toward the upper and the lower parts of the mixing region. Thus at sufficiently high Ω and a/D, we can observe the distortions of the tracer which are almost symmetrical with respect to $y = 0$. The example of such a shape of the tracer is presented in figure 17(b) for $\Omega = 2.33$, $a/D = 0.45$, $\tau = 15$. As Ω and a/D decrease, the intensity

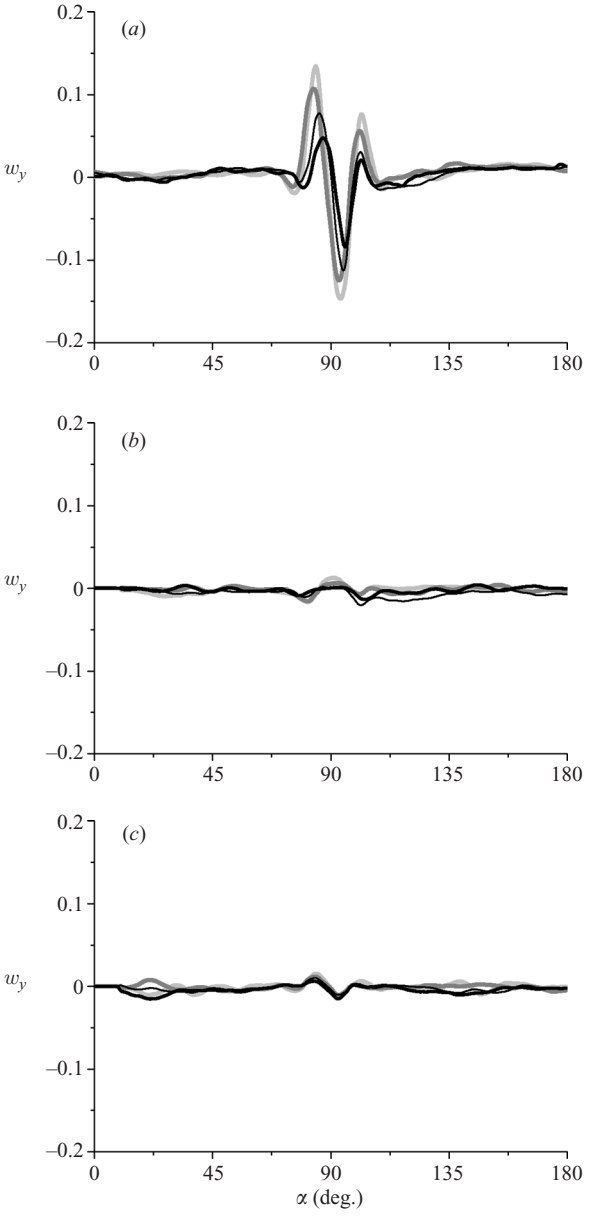

FIGURE 16. Profiles of $w_y(\alpha)$ in the cases of circular, horizontal and vertical oscillations at $\Omega > 1$. All profiles are taken at fixed non-dimensional time $\tau = 12$ and fixed value of the amplitude $a/D = 0.3$: thick black, thin black, grey and light grey lines correspond to (*a*) $\Omega = 1.17, 1.4, 1.89, 2.33$, (*b*) $\Omega = 1.27, 1.55, 1.89, 2.59$ (*c*) $\Omega = 1.23, 1.55, 1.89, 2.59$.

of the currents associated with the production of mixed fluid and the vertical collapse of the mixed region strongly decreases, and we observe the tracer distortions similar to those depicted in figures 11(*a*) and 17(*a*).

A study on dynamics of mixing and formation of nearly horizontal interfaces by long-term orbital motion of a circular cylinder as well as the detailed study of the regimes similar to that depicted in in figure 17(*b*) fall out of the scope of the present

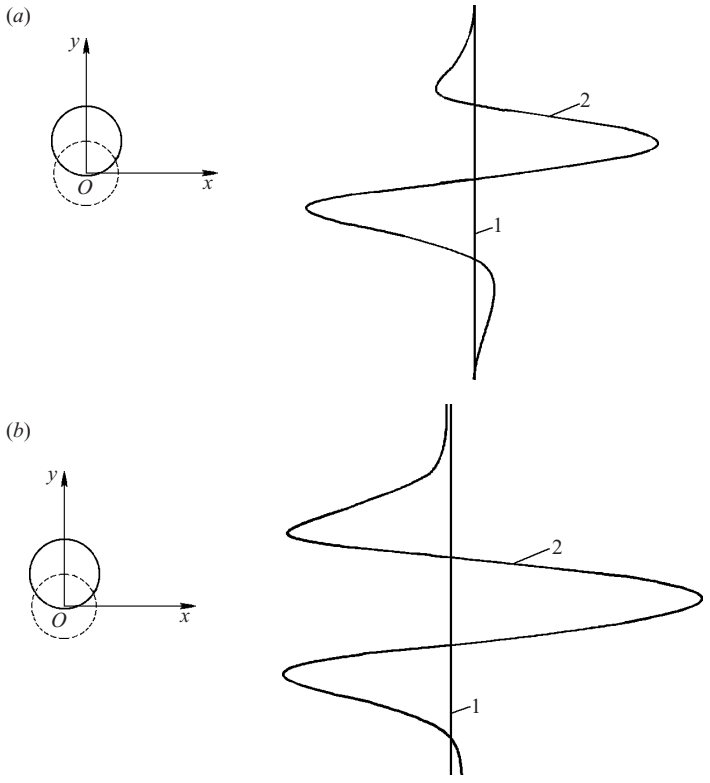

FIGURE 17. Horizontal currents induced by clockwise circular oscillations of the cylinder. Dashed line shows the circular orbit of the cylinder centre. Oscillation amplitude for both images is $a/D = 0.45$. Lines 1 correspond to $\tau = 0$. (*a*) $\Omega = 1.17$, line 1 is located at distance $8D$ from the point O, line 2 corresponds to $\tau = 20$ (*b*) $\Omega = 2.33$, line 1 is located at distance $7.5D$ from the point O, line 2 corresponds to $\tau = 15$

paper. There exists an extensive literature on mixing of a continuously stratified fluid by different mechanical stirring devices. Discussion of typical experimental configurations and relevant theoretical analysis can be found, for example, in Hopfinger (1987) and Balmforth, Smith & Young (1998). Some parallels can be drawn between the present results and the effects described in the literature on mixing, in particular, in experimental works on collapse of the mixing region (starting with the pioneering study by Wu 1969) and the studies where stirring is applied at a boundary and the layers are extruded into the surrounding non-turbulent fluid (Ivey & Corcos 1982; Thorpe 1982). A distinguishing feature of the present experiments is that the orbital motion of the cylinder represent an isolated stirring event generating nearly horizontal currents with a non-zero total angular momentum. Also, the frequency of oscillation in the present experiments remains comparable with the buoyancy frequency ($\Omega < 3$) while in the major part of the 'mixing box' experiments $\Omega > 10$. Such an isolated stirring event may be of interest as a model of more complicated currents with a non-zero total angular momentum.

4. Conclusion

In this work we have performed a comparative experimental study of internal waves generated by large-amplitude circular and rectilinear oscillations of a circular cylinder

in a uniformly stratified fluid. The inviscid mechanics of internal wave generation by circular oscillations of a circular cylinder has been considered in Hurley & Hood (2001). Linear analysis shows that small circular oscillations in a clockwise direction generate internal waves only in the beams passing through the first and third quadrants of the Cartesian coordinate system.

In agreement with the linear scenario, at small amplitude of clockwise circular oscillations ($a/D = 0.15$) we observe internal wave beams in the first and third quadrants. The intensity of these waves is approximately twice the intensity of waves radiated by purely horizontal or vertical oscillations. The shapes of the wave envelopes in the cases of small-amplitude circular, horizontal and vertical oscillations remain by and large similar. Weak nonlinear effects, in particular, (i) generation of a density-gradient perturbation at 'zero frequency', and (ii) wave radiation into the second and third quadrants, are already detectable for orbital motion at $a/D = 0.15$. These effects drastically increase with the motion amplitude.

In a viscous uniformly stratified fluid with no-slip condition at the body surface, circular and rectilinear oscillations represent different stirring events. Visualization shows that the typical size of the stirring region in the case of circular oscillations is much greater than in the case of rectilinear oscillations of the same magnitude. This intense stirring serves as an additional dissipative mechanism. As a result, the intensity of wave motion generated by large-amplitude ($a/D = 0.3; 0.45$) circular oscillations in the main beams is no longer twice the intensity of waves generated by horizontal or vertical oscillations. It drops below the value that might be anticipated in a linear case. At large oscillation amplitudes there is also a notable difference between the shapes of wave envelopes in the cases of circular and rectilinear oscillations.

Evolution of the secondary wave beams passing through the second and fourth quadrants is believed to be related to the processes in the stirring region. It is shown that, in general, circular oscillations tend to generate disturbances evolving on longer time scale than the disturbances generated by rectilinear oscillations.

When $\Omega < 0.5$ (i.e. the frequency of oscillations is smaller than half of the buoyancy frequency), nonlinear radiation of waves with frequency 2Ω is possible. Our experimental results show that waves with frequency 2Ω follow the same trend as waves with frequency Ω: in the case of clockwise circular oscillations, waves are primarily radiated into the first and third quadrants of the Cartesian coordinate system.

Flow visualization shows that circular oscillations generate 'zero-frequency' disturbance (which can be interpreted as a specific kind of a columnar mode) associated with the mass-transfer current induced by the cylinder motion. This mass-transfer current has a non-zero value of the total angular momentum with respect to the centre of the cylinder trajectory. The magnitude of the density-gradient perturbation at zero frequency grows continuously. It does not reach a saturated value over the typical time of experimental observations (from 20 to 30 periods). There are reasons to believe that the mass-transfer currents induced by the orbital motion of the cylinder ultimately lead to the formation of a layered structure. In the present study, the long-term evolution has not been investigated because of inevitable difficulties associated with the limited horizontal size of the test tank.

The authors are grateful to the referees for their constructive comments. Thanks are due to I. V. Sturova for discussions and to B. Voisin for discussions and interesting scientific correspondence. Inventive mechanical work of E. M. Romanov and technical help of V. A. Kostomakha are gratefully acknowledged. This study was partially

Displacement (mm)	Measurement error (%)	Standard deviation (%)
0.1	−15	±7
0.3	−8	±5
0.7	−5	±4
1.1	−4.5	±3
1.7	−1.8	±2
2.8	−1	±1.6

TABLE 2. The results of preliminary tests on the measurement accuracy.

supported by Integration program of departments of RAS (project 4.14.1) and by RFBR-CNRS (project 07-01-92212). The major revision of the paper was prepared during the stay of E.V.E. as a visiting professor at LEGI, Grenoble.

Appendix. Accuracy of the displacement field measurements

The Dantec Flowmanager software is known to be a reliable tool for cross-correlation analysis. A comparison of the software performance shown by different commercially available PIV systems is given in Adrian (2005). The early history of the method is reviewed in Adrian (1991).

In the present work, the accuracy of the displacement field calculation was tested by introducing small prescribed translational and angular displacements of the screen with the help of micrometric screws. In an ideal system, a uniform vertical translation of the screen would produce identical measurements of vertical displacements in all interrogation areas. In reality, owing to thermal and electronic noise, the measurement results have a scatter with respect to the mean value averaged over all interrogation areas. Also, the mean measured value itself may yield a biased estimate. The results of our tests for a set of uniform vertical displacements, with associated systematic errors and standard deviations, are summarized in table 2. The camera was located 350 cm from the screen, with the field of view $65 \times 45\,\mathrm{cm}^2$. In experiments with internal waves, the typical measured apparent displacements were of order 1 mm, corresponding to the acceptable level of measurement errors. The effects discussed in the paper are well beyond the possible uncertainty of measurements.

It is worth making some comments on the long-term drift which is typically present in the synthetic schlieren measurements (see Sutherland & Linden 2002). In some series of our experiments, the drift was observable at the lowest amplitude $a/D = 0.15$ of the cylinder oscillations. The experiments with the lowest amplitude were repeated several times and the series with the minimum drift were selected for further analysis. At higher a/D, the drift-to-signal ratio was very small. One reason for small drifts in the present experiments is related to higher value of γ in sugar–water solutions as compared to salt solutions. The internal waves of equal amplitudes in sugar- and salt-stratified fluids with the same value of the buoyancy frequency produce roughly 1.5 times stronger optical distortions in the case of sugar stratification. The other reason may be related to small overall temperature variations in the laboratory located in the basement of the building, where the experiments were performed. Care was taken to minimize thermal convective currents related to the presence of people, and measuring and analysing devices.

REFERENCES

Adrian, R. J. 1991 Particle-imaging techniques for experimental fluid dynamics. *Annu. Rev. Fluid. Mech.* **23**, 261–304.

Adrian, R. J. 2005 Twenty years of particle image velocimetry. *Exps. Fluids* **23**, 261–304.

Baidulov, V. G. & Chashechkin, Yu. D. 1993 The diffusion effect on the boundary flow in a continuously stratified fluid. *Izv. Atmos. Ocean. Phys.* **29**, 641–647.

Baidulov, V. G. & Chashechkin, Yu. D. 1996 A boundary current induced by diffusion near a motioness horizontal cylinder in a continuously stratified fluid. *Izv. Atmos. Ocean. Phys.* **32**, 751–756.

Balmforth, N. J., Smith, S. G. L. & Young, W. R. 1998 Dynamics of interfaces and layers in a stratified turbulent fluid. *J. Fluid Mech.* **355**, 329–358.

Batchelor, G. K. 1967 *An Introduction to Fluid Dynamics*. Cambridge University Press.

Bronshtein, I. N., Gurov, K. P., Kuznetsov, E. B. 1959 *A Short Physical–Technical Handbook*, vol. 1. Gos. Izdat. Fiz. mat. Lit. (in Russian), Mosow.

Dalziel, S. B. 2000 Synthetic schlieren measurements of internal waves generated by oscillating a square cylinder. *Proc. 5th Intl Symp. on Stratified Flows, Vancouver, Canada, 10–13 July 2000*, vol. 2, pp. 743–748. University of British Columbia, Vancouver.

Dalziel, S. B., Hughes, G. O. & Sutherland, B. R. 2000 Whole field density measurements by 'synthetic' schlieren. *Exps. Fluids* **28**, 322–335.

Dean, W. R. 1948 On the reflection of surface waves by a submerged circular cylinder. *Proc. Camb. Phil. Soc.* **44**, 483–491.

Ermanyuk, E. V. 2000 The use of impulse response functions for evaluation of added mass and damping coefficient of a circular cylinder oscillating in a linearly stratified fluid. *Exps. Fluids* **28**, 152–159.

Ermanyuk, E. V. & Gavrilov, N. V. 2001 Force on a body in a continuously stratified fluid. Part 1. Circular cylinder. *J. Fluid Mech.* **451**, 421–443.

Ermanyuk, E. V. & Gavrilov, N. V. 2005 Duration of transient processes in the formation of internal-wave beams. *Dokl. Phys.* **50**, 548–550.

Ermanyuk, E. V. & Gavrilov, N. V. 2007 A note on the propagation speed of a weakly dissipative gravity current. *J. Fluid Mech.* **574**, 393–403.

Flynn, M. R., Onu, K. & Sutherland, B. R. 2003 Internal wave excitation by a vertically oscillating sphere. *J. Fluid Mech.* **494**, 65–93.

Garrett, C. & Kunze, E. 2007 Internal tide generaton in the deep ocean. *Annu. Rev. Fluid Mech.* **39**, 57–87.

Gavrilov, N. V. & Ermanyuk, E. V. 1997 Internal waves generated by circular translational motion of a cylinder in a linearly stratified fluid. *J. Appl. Mech. Tech. Phys.* **38**, 224–227.

Gostiaux, L. & Dauxois, T. 2007 Laboratory experiments on the generation of internal tidal beams over steep slopes. *Phys. Fluids* **19**, 028102.

Gostiaux, L., Didelle, H., Mercier, S. & Dauxois, T. 2007 A novel internal waves generator. *Exps. Fluids* **42**, 123–130.

Hopfinger, E. J. 1987 Turbulence in stratified fluids: a review. *J. Geophys. Res.* **92**, 5287–5303.

Hurley, D. G. 1997 The generation of internal waves by vibrating elliptic cylinders. Part 1. Inviscid solution. *J. Fluid Mech.* **351**, 105–118.

Hurley, D. G. & Keady, G. 1997 The generation of internal waves by vibrating elliptic cylinders. Part 2. Approximate viscous solution. *J. Fluid Mech.* **351**, 119–138.

Hurley, D. G. & Hood, M. G. 2001 The generation of internal waves by vibrating elliptic cylinders. Part 3. Angular oscillations and comparison of theory with recent experimental observations. *J. Fluid Mech.* **433**, 61–75.

Ivey, G. N. & Corcos, G. M. 1982 Boundary mixing in a stratified fluid. *J. Fluid Mech.* **121**, 1–26.

Linden, P. F. & Weber, J. E. 1977 The formation of layers in a double-diffusive system with a sloping boundary. *J. Fluid Mech.* **81**, 757–773.

Longuet-Higgins, M. S. 1970 Steady currents induced by oscillations round islands. *J. Fluid Mech.* **42**, 701–720.

Mowbray, D. E. & Rarity, B. S. H. 1967 A theoretical and experimental investigation of the phase configuration of internal waves of small amplitude in a density-stratified fluid. *J. Fluid Mech.* **28**, 1–16.

Ogilvie, T. F. 1963 First- and second-order forces on a cylinder submerged under a free surface. *J. Fluid Mech.* **16**, 451–472.

Onu, K., Flynn, M. R. & Sutherland, B. R. 2003 Schlieren measurement of axisymmetric internal wave amplitudes. *Exps. Fluids* **35**, 24–31.

Peacock, T. & Tabaei, A. 2005 Visualiation of nonlinear effects in reflecting internal wave beams. *Phys. Fluids* **17**, 061702.

Phillips, O. M. 1970 On flows induced by diffusion in a stably stratified fluid. *Deep-Sea Res.* **17**, 435–443.

Riley, N. 1971 Stirring of a viscous fluid. *Z. Angew. Math. Phys.* **22**, 645–653.

Scase, M. M. & Dalziel, S. B. 2006 Internal wave fields generated by a translating body in a stratified fluid: experimental comparison. *J. Fluid Mech.* **564**, 305–331.

Sturova, I. V. 1994 Plane problem of hydrodynamic rocking of a body submerged in a two-layer fluid without forward speed. *Fluid Dyn.* **29**, 414–423.

Sturova, I. V. 1999 Problems of radiation and diffraction for a circular cylinder in a stratified fluid. *Fluid Dyn.* **34**, 521–533.

Sutherland, B. R. & Linden P. F. 2002 Internal wave excitation by a vertically oscillating elliptic cylinder. *Phys. Fluids* **14**(2), 721–739.

Sutherland, B. R., Dalziel, S. B., Hughes, G. O. & Linden, P. F. 1999 Visualization and measurement of internal waves by 'synthetic' schlieren. Part 1. Vertically oscillating cylinder. *J. Fluid Mech.* **390**, 93–126.

Sutherland, B. R., Hughes, G. O., Dalziel, S. B. & Linden, P. F. 2000 Internal waves revisited. *Dyn. Atmos. Oceans* **31**, 209–232.

Thorpe, S. A. 1982 On the layer produced by rapidly oscillating a vertical grid in a uniformly stratified fluid. *J. Fluid Mech.* **124**, 391–409.

Turner, J. S. 1973 *Buoyancy Effects in Fluids.* Cambridge University Press.

Ursell, F. 1950 Surface waves in the presence of a submerged circular cylinder, I and II. *Proc. Camb. Phil. Soc.* **46**, 141–158.

Vargaftik, N. B. 1963 *Handbook on the Thermophysical Properties of Gases and Liquids.* Gos. Izdat. Fiz.-Mat. Lit. (in Russian). Moscow.

Vlasenko, V., Stashchuk, N., Hutter, K. 2005 *Baroclinic Tides. Theoretical Modeling and Observational Evidence.* Cambridge University Press.

Voisin, B. 2003 Limit states of internal wave beams. *J. Fluid Mech.* **496**, 243–293.

Westerweel, J. 1997 Fundamentals of digital particle image velocimetry. *Meas. Sci. Technol.* **8**, 1379–1392.

Wu, J. 1969 Mixed region collapse with internal wave generation in a density-stratified medium. *J. Fluid Mech.* **35**, 531–544.

Wunsch, C. 1970 On oceanic boundary mixing. *Deep-Sea Res.* **17**, 293–301.

Xu, Y., Boyer, D. L., Fernando, H. J. S. & Zhang, X. 1997 Motion fields generated by the oscillatory motion of a circular cylinder in a linearly stratified fluid. *Expl Thermal Fluid Sci.* **14**, 277–296.